



PERGAMON

Continental Shelf Research 22 (2002) 1129–1151

---

---

CONTINENTAL SHELF  
RESEARCH

---

---

www.elsevier.com/locate/csr

## High resolution modeling and data assimilation in the Monterey Bay area

I. Shulman<sup>a,\*</sup>, C.-R. Wu<sup>a</sup>, J.K. Lewis<sup>b</sup>, J.D. Paduan<sup>c</sup>, L.K. Rosenfeld<sup>c</sup>,  
J.C. Kindle<sup>d</sup>, S.R. Ramp<sup>c</sup>, C.A. Collins<sup>c</sup>

<sup>a</sup>COAM, University of Southern Mississippi, Stennis Space Center, Building 1103, Room 249, MS 39529, USA

<sup>b</sup>Scientific Solution, Inc., Kalaheo, HI, USA

<sup>c</sup>Naval Postgraduate School, Monterey, CA, USA

<sup>d</sup>Naval Research Laboratory, Stennis Space Center, MS, USA

Received 13 September 2000; received in revised form 2 October 2001; accepted 15 October 2001

---

### Abstract

A high resolution, data assimilating ocean model of the Monterey Bay area (ICON model) is under development within the framework of the project “An Innovative Coastal-Ocean Observing Network” (ICON) sponsored by the National Oceanographic Partnership Program. The main objective of the ICON model development is demonstration of the capability of a high resolution model to track the major mesoscale ocean features in the Monterey Bay area when constrained by the measurements and nested within a regional larger-scale model.

This paper focuses on the development of the major ICON model components, including grid generation and open boundary conditions, coupling with a larger scale, Pacific West Coast (PWC) model, atmospheric forcing etc. Impact of these components on the Model’s predictive skills in reproducing major hydrographic conditions in the Monterey Bay area are analyzed.

Comparisons between observations and the ICON model predictions with and without coupling to the PWC model, show that coupling with the regional model improves significantly both the correlation between the ICON model and observed ADCP currents, and the ICON model’s skill in predicting the location and intensity of observed upwelling events.

Analysis of the ICON model mixed layer depth predictions show that the ICON model tends to develop a thicker than observed mixed layer during the summer time, and while assimilation of sea surface temperature data is enough for development of observed thin mixed layer in the regional larger-scale model, the fine-resolution ICON model needs variable heat fluxes as surface boundary conditions for the accurate prediction of the vertical thermal structure.

The paper targets researchers involved in high-resolution numerical modeling of coastal areas in which the dynamics are determined by the complex geometry of a coastline, variable bathymetry and by the influence of complex water masses from a complicated hydrographic system (such as the California Current system). © 2002 Elsevier Science Ltd. All rights reserved.

*Keywords:* Hydrodynamics; Coastal currents; Upwelling; HF Radars; Numerical modeling; Data assimilation; USA; California; Monterey Bay

---

\*Corresponding author. Fax: +1-228-6887072.

E-mail address: shulman@coam.usm.edu (I. Shulman).

## 1. Introduction

The Monterey Bay is the largest bay of the West Coast of the United States and is recognized nationally as a National Marine Sanctuary. This region is characterized by a complex coastline and regions of steep topography. Local upwelling events and strong land/sea breeze influence circulation patterns in this area. During spring and summer, near-surface water offshore of the Monterey Bay flows mostly southward due to local equatorward wind stress and the influence of the California Current (CC) (see, Rosenfeld et al., 1994). According to Ramp et al. (1997) and Collins et al. (2000), there are two narrow, poleward flowing boundary currents around the Monterey Bay area: the Inshore Countercurrent (IC) (sometimes called the Davidson Current), and the California Undercurrent (CU). The water properties of the CC, IC and CU currents are determined by four water masses (Lynn and Simpson, 1987): the Pacific Subarctic (in upper 200 m), the North Pacific Central and Coastal Upwelled water masses and, in the subsurface, by the Equatorial Pacific. Tidal observations in this area (Petruncio et al., 1998; Paduan and Rosenfeld, 1996) show sea surface fluctuations characterized by a mixed, predominantly semidiurnal tide with the largest constituent being the “M2” tide and the second largest being the “K1”. Analysis of the surface current data derived from HF radar (CODAR) and CTD observations indicated a presence of large internal tides in the Monterey Canyon.

All above mentioned atmospheric and oceanographic conditions and processes make the Monterey Bay area very interesting for numerical modeling. A numerical study of barotropic and internal tides has been reported in Petruncio (1996) and Rosenfeld et al. (1999). Modeling of the Monterey Bay region response to wind forcing and tides has been studied by Ly et al. (1999), development of nowcasts of the surface currents by blending CODAR data and model velocities is reported in Lipphardt et al. (1997, 2000). Modeling of the tidal and wind driven flow with assimilation of CODAR derived surface currents can be found in our previous study (Lewis et al., 1998).

The development of an assimilation scheme for CODAR-derived surface current data was the major objective of the Lewis et al. (1998) study. The CODAR surface current data assimilation technique was based on the application of a pseudo-shearing stress over the surface layer of the model. This pseudo-shearing stress depended on the differences between the model-predicted velocities and the velocities observed by the HF Doppler system. Testing and evaluation of the proposed data assimilation scheme were conducted over 10 days of simulations in August, 1994, by using the Monterey Bay model forced with a uniform wind and tidal surface height amplitudes and phases from the global tidal model of Schwiderski.

In the present paper, following the objectives of the “Innovative Coastal-Ocean Observing Network” (ICON) project, we discuss and evaluate the ICON model features which are needed for modeling major mesoscale phenomena, including eddies and upwelling filaments, in the Monterey Bay area. A separate paper will be devoted to the CODAR data assimilation issues which represent another major objective of the ICON project. Also, the ICON model design has a long-term purpose in the development of a realistic coastal circulation model for a nowcast/forecast prediction modeling system in and around the Monterey Bay area.

The ICON model configuration will be discussed throughout the paper; here in the introduction, we would like to highlight some of the important issues of the ICON model development.

(a) In order to include the influence of the CC, CU, and IC on the flow regime and water properties, the ICON model open boundary conditions are derived from the predictions of the larger-scale Pacific West Coast (PWC) model (Clancy et al., 1996; Ko et al., 1996; Righi et al., 1999; Rochford and Shulman, 2000). Also, the coupling of coastal models to larger-scale models is important for the development of successful data assimilation schemes with coastal models. Assimilated data (for example, CODAR measurements) are influenced by physical processes deter-

mined by the larger-scale phenomena generated outside of the limited-area coastal model. In this case, without coupling to a basin scale model, the assimilation process might result in the generation of transient waves, which cannot propagate out of the coastal model domain.

The coupling scheme for the ICON and PWC models is discussed in Section 2, and in Section 4, the significance and importance of the coupling with the larger-scale PWC model will be demonstrated by a comparison of the ICON model predictions with and without coupling.

(b) Specification of open boundary conditions remains one of the main challenges in coastal model development. For the successful implementation of open boundary conditions, the orientation of coastal model boundaries is very important. Most existing radiation-type open boundary conditions work well in the case when flow is almost orthogonal to the open boundaries (the tangential component is not significant). However, for coastal limited-area models, the tangential component of flow can be significant if the open boundaries are oriented parallel to the longitude and latitude (for cartesian, rectangular grids). In this case, specification of the tangential component of the flow, with or without the use of extraneous information (for example, from a larger-scale model) can introduce significant unrealistic currents around the open boundaries. In order to overcome this problem in our present study, the ICON model domain (Fig. 1) has an orthogonal, curvilinear grid with cross-shelf open boundaries that are nearly orthogonal to the isobaths of bathymetry—in order for the flow to be almost normal to the open boundaries.

The paper has the following structure: in Section 2 we outline the model along with the forcing and formulations; observational data used for comparisons with the ICON model predictions are described in Section 3. In Section 4, we present the results of model runs and compare these with observations. Section 5 presents a discussion of, and future plans for, model development. Note that some early stages of the ICON model development can be found in Shulman et al. (1999).

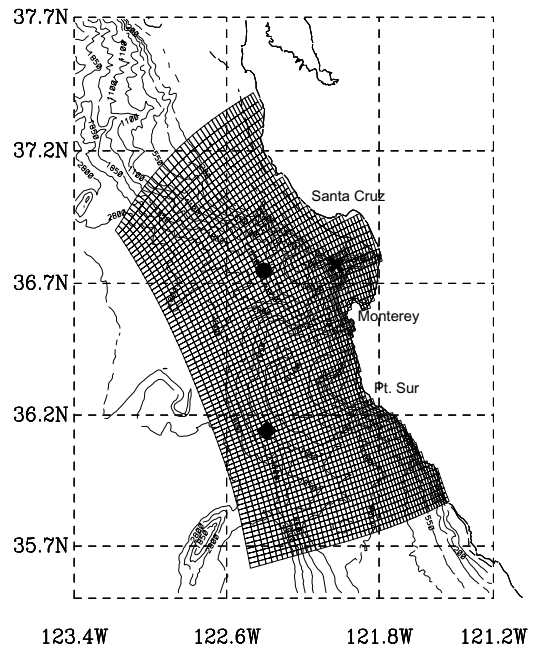


Fig. 1. Model grid and bathymetry. Locations of moorings M1, M2 and M4 are marked by “x”, circle and diamond, correspondingly.

## 2. Monterey Bay area model (ICON)

The orthogonal, curvilinear grid and model bathymetry are presented in Fig. 1. The grid has a variable resolution in the horizontal, ranging from 1 to 4 km, with finer-resolution around the Bay. The model has 30 vertical sigma levels. Cross-shelf open boundaries of the model (northern and southern) are approximately orthogonal to the isobaths of bathymetry in order for the flow to be almost perpendicular to the cross-shelf open boundaries. A three-dimensional, sigma-coordinate version of the Blumberg and Mellor (1987) hydrodynamic model was used. This three-dimensional, free surface model is based on the primitive equations for momentum, salt, and heat. It uses the turbulence closure sub-model developed by Mellor and Yamada, and the Smagorinsky formulation is used for horizontal mixing. Additional information on the model can be found in Blumberg and Mellor (1987).

On the open boundaries, the ICON model is one-way coupled to a larger-scale PWC model.

The PWC model is also based on the Blumberg and Mellor model (explicit, sigma-coordinate version) and has a horizontal resolution of  $\frac{1}{12}^\circ$  (around 10 km) and 30 vertical sigma levels. The PWC model domain extends seaward to  $135^\circ\text{W}$  longitude, and from  $30^\circ\text{N}$  to  $49^\circ\text{N}$  in latitude. The model includes seven major rivers and is forced with wind products from Navy Operational Global Atmospheric Prediction System (NOGAPS) and Navy Coupled Ocean and Atmospheric Mesoscale Prediction System (COAMPS) (Hodur, 1997) models predictions. The model assimilates sea surface temperature (SST) from daily predictions of Multi-Channel Sea Surface Temperature (MCSST). An important feature of the PWC model is a coupling to a  $\frac{1}{4}^\circ$ , global Navy Layered Ocean Model (NLOM) which has an assimilating capability for altimeter sea surface height observations.

The Blumberg and Mellor model uses the so-called mode splitting technique, where the separation of the vertically integrated governing equations (barotropic, external mode) and the equations governing vertical structure (baroclinic, internal mode) is introduced. Boundary conditions are formulated for the barotropic and baroclinic modes separately and then adjusted to take into account the different truncation errors for those modes (Blumberg and Mellor, 1987).

There is one-way coupling between the PWC and the NLOM (Ko et al., 1996; Rochford and Shulman, 2000), with sea surface height and transport from the NLOM model predictions used to prescribe the open boundary conditions for the barotropic mode of the PWC model. For the baroclinic mode, information from the NLOM model is not used: radiation condition for velocities and climatological temperature and salinity were used for the baroclinic open boundary conditions of the PWC model.

The one-way coupling between the ICON and PWC models is described below. The barotropic, vertically averaged velocities on the open boundaries of the Monterey Bay area model were estimated by using the Flather (1976) formulation:

$$\bar{u}_n = \bar{u}_n^o + (g/H)^{1/2}(\eta - \eta^o), \quad (1)$$

where  $u_n$  is the vertically averaged outward normal component of the velocity on the open boundary at time  $t$ ;  $\bar{u}_n^o$  is the outward vertically averaged normal component of the velocity on the open boundary at time  $t$  estimated from the PWC model results;  $\eta$  is the model sea surface elevation calculated from the continuity equation and located half of a grid inside of the open boundary in the ICON model domain;  $\eta^o$  is the PWC model sea surface elevation on the open boundary of the Monterey Bay area model;  $H$  is the water depth on the open boundary, and  $g$  is gravitational acceleration. At the same time, an adjustment procedure was used to balance the net transport from the PWC model with the associated variation of sea surface elevation. The available outputs from the PWC model have daily records of sea surface elevation and transports; they were spatially interpolated to the ICON grid by using bivariate interpolation and were linearly interpolated to the ICON model time step in order to form  $\eta^o$  and  $\bar{u}_n^o$  in the formulation (1). As a result, there is a lack of continuity between the total transport through the open boundaries estimated from  $\bar{u}_n^o$  and the total change in the sea surface elevation of the modeling area estimated from  $\eta^o$ . To balance these records, any difference was added to the values of  $\bar{u}_n^o$  along the open boundaries, those additions were inversely proportional to the water depth at any particular location on the open boundaries. For the tangential component of the velocity, an advectational boundary condition is used:

$$\frac{\partial \bar{u}_\tau}{\partial t} + \bar{u}_n \frac{\partial \bar{u}_\tau}{\partial n} = 0,$$

where here

$$\frac{\partial \bar{u}_\tau}{\partial n} = \begin{cases} (\bar{u}_r - \bar{u}_\tau^o)/\delta x_n & \bar{u}_n \geq 0 \\ (\bar{u}_{i,\tau} - \bar{u}_\tau)/\delta x_n & \bar{u}_n < 0 \end{cases},$$

where  $\bar{u}_\tau$  is the tangential component of vertically averaged velocity on the open boundary at time  $t$ ;  $\bar{u}_{i,\tau}$  is the tangential component of vertically averaged velocity at one grid point inside of the open boundary;  $\bar{u}_\tau^o$  the tangential component of vertically averaged velocity on the open boundary at time  $t$  estimated from the PWC model results and  $\delta x_n$  the grid spacing in the direction normal to the boundary. According to the advectational open

boundary condition, the vertically averaged tangential component of velocity from the PWC model is advected into the model domain in the case of inflow, and the internal, vertically averaged, tangential component of velocity is advected to the open boundary in the case of out-flow. For temperature and salinity on the open boundaries, the advective boundary conditions were used; advected values were calculated from the PWC profiles of temperature and salinity, and interpolated to the ICON model grid. Baroclinic velocities for the ICON model have been determined from a radiation condition for the normal component and advective boundary condition for the tangential component of the velocity.

The ICON model was initialized in June 1994 with a horizontally constant vertical profile of temperature and salinity based on summer conditions in the Bay. The model was forced with the FNMOC NOGAPS 12-h surface wind stresses and coupled (as described above) at the open boundaries to the PWC model. The model was run for 1994–1999 period.

### 3. Data

In Section 4, the ICON model predictions are compared with observed data which are described in this section.

Correlations are calculated between model results and currents measured by a 300 kHz RD Instruments Acoustic Doppler Current Profiler (ADCP) mounted in a downward-looking configuration on the Monterey Bay Aquarium Research Institute's (MBARI) surface mooring at 122.40°W, 36.67°N, designated M2 (see Fig. 1). For the three months of data used here (June 1–August 31, 1999), the ADCP was set up to measure in 4-m depth bins and generally returned good data in the depth range from 6 to 120 m. Horizontal velocity data are ensemble averages made every 2 h from 180 pings emitted every second, yielding a manufacturer's stated accuracy of 0.2 cm/s. To minimize the effect of surface wave motion on the measurement, the pitch and roll data were not used in the transformation of velocity to earth coordinates, nor in the bin

mapping. Contamination of the measured velocity due to surface wave motion is estimated to cause errors of only about 1 cm/s in the ensemble-averaged earth-referenced velocity. Horizontal motion due to the mooring's wander within its watch circle has not been subtracted, but based on GPS measurements of the mooring position made at 15 or 30-min intervals on a similar mooring nearby, it has been estimated to generally be <3–4 cm/s.

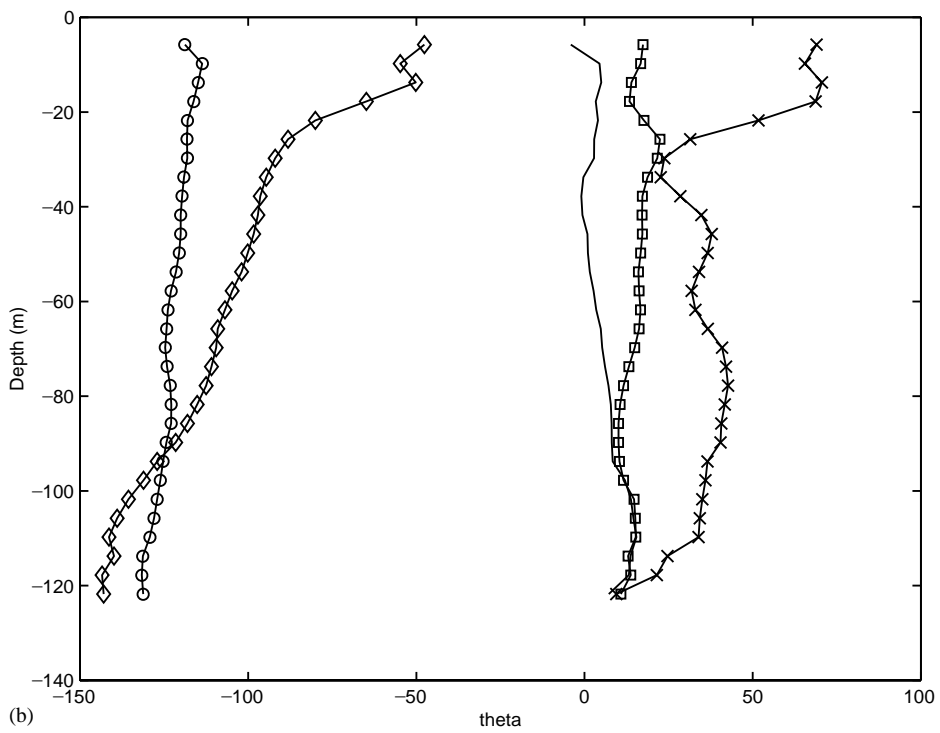
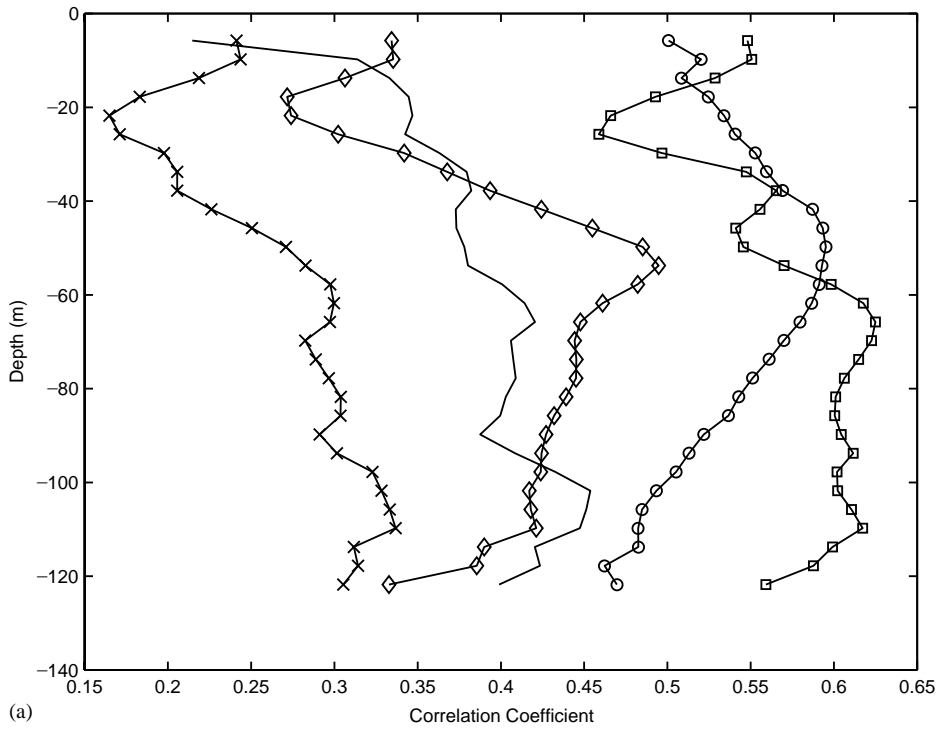
Model temperatures and salinities are compared with those measured by Sea-Bird MicroCAT CTDs mounted on MBARIs M1 (122.02°W, 36.74°N) and M2 and ICONs M4 (122.43°W, 36.15°N) (Fig. 1) surface moorings. The instruments were calibrated before the deployments which lasted approximately 1 yr. The manufacturer's stated accuracy and drift rate for temperature (conductivity) are 0.002° (0.003 mS/cm) and 0.0002°/month (0.003 mS/cm/month), respectively, so the instantaneous data are expected to be accurate to within about 0.005°C and 0.006 psu. Comparisons of the moored MicroCAT data with adjacent shipboard profiles made with a Sea-Bird SBE-19, show agreement to generally be within 0.1°C and 0.01 psu. One-hour averages of one instantaneous sample per 10 min were low-pass filtered with a 33-h cut-off.

### 4. Model simulations results

First, we evaluate the value added to the ICON model predictions by the coupling between ICON and PWC models. Three ICON model test runs are compared.

In Test 0, the information from the PWC model was not used for specification of open boundary conditions of the ICON model. Radiation conditions for barotropic, and baroclinic layer velocities, and climatological temperature and salinity (instead of PWC temperature and salinity fields), were used for specification of the ICON model open boundary conditions.

In Test 1, only the barotropic information from the PWC (sea surface height and transport) was used to specify open boundary conditions for the ICON model in the formulation (1). For the



baroclinic mode, open boundary conditions were specified in accordance with the Test 0 case; therefore information from the PWC model was not used for specification of baroclinic open boundary conditions of the ICON model.

Finally, in Test 2 the baroclinic, as well as barotropic information from the PWC model predictions was used to specify open boundary conditions for the ICON model according to the coupling scheme outlined in Section 2.

To estimate the value added to the ICON model predictions by coupling with the PWC model, the ICON model test runs with and without coupling to the PWC model were compared with ADCP currents at buoy M2.

The magnitudes of complex correlation coefficients and the angular displacements between the ADCP and ICON model currents at buoy M2 were calculated according to Kundu (1976). The magnitude  $\rho$  of complex correlation coefficient between the ADCP and ICON model currents for a particular depth is estimated by using the following formula:

$$\rho = \sqrt{Re^2 + Im^2},$$

where

$$Re = \frac{\sum_t (u_t^o u_t^m + v_t^o v_t^m)}{\sqrt{\sum_t ((u_t^o)^2 + (v_t^o)^2) \sum_t ((u_t^m)^2 + (v_t^m)^2)}}$$

$$Im = \frac{\sum_t (u_t^o v_t^m - v_t^o u_t^m)}{\sqrt{\sum_t ((u_t^o)^2 + (v_t^o)^2) \sum_t ((u_t^m)^2 + (v_t^m)^2)}}$$

The corresponding angular displacement  $\theta$  (phase angle, average veering) for particular depth is

estimated according to:

$$\theta = \tan^{-1} \frac{\sum_t (u_t^o v_t^m - v_t^o u_t^m)}{\sum_t (u_t^o u_t^m + v_t^o v_t^m)},$$

where  $u_t^m, v_t^m$  and  $u_t^o, v_t^o$  are demeaned model and observed east–west and north–south components of velocity.  $\theta$  gives the average counterclockwise angle of the ICON currents with respect to the ADCP currents. The magnitudes of correlation coefficients and angles as a function of depth are estimated for the period of the summer of 1999 and presented in Figs. 2a and b.

The line marked with circles represents the magnitude of the complex correlation  $\rho$  (Fig. 2a) and angle  $\theta$  (Fig. 2b) for the Test 0 run when the ICON model was not coupled to the PWC model. In this case, while the amplitude of the correlation is fairly high, the average angles between the ICON model currents and M2 currents are larger than  $100^\circ$  for the top 120 m, which indicates that on average the currents from Test 0 and M2 are pointing in opposite directions. The solid line marked with “ $\times$ ” represents the magnitude of the complex correlation (Fig. 2a) and angles (Fig. 2b) between the PWC model and M2 currents. The magnitude of the complex correlation between PWC and M2 currents is much lower than the magnitude of the complex correlation between currents from Test 0 and M2. However, for all depths the average angles between the PWC and M2 currents are around  $50^\circ$  and are less than half the average angles between Test 0 run and M2 currents. In this case, we might expect that the coupling of the ICON model with the PWC model (Tests 1 and 2) should decrease the average angle between the ICON model and M2 currents; however the magnitude of complex correlation might also be decreased in the case of coupling. This is exactly what can be seen in Fig. 2, where the magnitudes of complex correlations (Fig. 2a) and average angles (Fig. 2b) for Tests 1 and 2 are presented by solid lines marked by diamonds and by unmarked solid lines, correspondingly. The use of only barotropic information from the PWC (Test 1) improved the average angle between the ICON model currents and observations. Finally, the barotropic and baroclinic coupling described in the previous section gives an almost zero

◀  
 Fig. 2. Magnitudes of complex correlation coefficients (a) and the angular displacements (b) between the ADCP and model-predicted currents at buoy M2. Solid unmarked lines are for the ICON model run from Test 2; solid lines marked with “ $\times$ ” are for the PWC model run; solid lines marked with circle are for the ICON model run from Test 0; solid lines marked with diamonds are for the ICON model run from Test 1. Finally, solid lines marked with squares are correlation coefficients and angular displacements between currents from the Test 2 ICON model run and PWC model.

average angle between the ICON model currents and observations, which is a significant improvement in the ICON model predictions in comparison to the case without coupling. The ICON model (solid unmarked lines) shows a higher correlation and smaller angle between the model and observed currents than the PWC model (solid line marked with “×”). This gives an estimate of the increase in the predictive skill of the ICON (finer-resolution) model in comparison to the PWC model. As might be expected due to the coupling of the ICON model with the PWC model, there is a high correlation and small veering between the ICON Test 2 run and PWC currents at the M2 location (lines marked with square in Figs. 2a and b).

Comparisons between modeled and observed SSTs for Tests 1 and 2 runs are presented in Fig. 3. The observed SSTs (Fig. 3, bottom panel) are reproduced significantly better in the results of Test 2 case simulation. This is obviously due to the use of the baroclinic signal from the records of the PWC model predictions. For example, in Test 2, cool plumes of upwelled water extend far north, up to the northern open boundary of the Monterey Bay model, which is not seen in the results of Test 1. The model reproduced a strong upwelling and, similar to prior observations (Rosenfeld et al., 1994), an offshore spreading of a cold water tongue can be seen in the southern portion of the Monterey Bay area. However, there is a lack of warm water in the northern part of the Bay. This discrepancy may be a result of a lack of surface heat fluxes at the air–sea interface of the ICON model.

In Figs. 4–6, the time series of 33-h low-pass filtered observed data and model-predicted (Test 2) temperatures and salinities for different depths are presented for stations M1, M2 and M4. The model results reproduced many of the observed trends in temperature and salinity. These include annual variations in temperature and salinity, cooling of surface and subsurface temperatures during spring upwelling, warming water masses during the summer and early fall, and cooling during late fall and winter.

The following quantitative parameters were used for the comparison of model-predicted and

observed temperatures and salinities for a given depth:

$$R = \frac{\sum_i (T_i^m - \overline{T^m})(T_i^o - \overline{T^o})}{\sqrt{\sum_i (T_i^m - \overline{T^m})^2} \sqrt{\sum_i (T_i^o - \overline{T^o})^2}}, \quad (2)$$

$$\sigma^{(m,o)} = \sqrt{\frac{\sum_i (T_i^{(m,o)} - \overline{T^{(m,o)}})^2}{N}}, \quad (3)$$

$$\varepsilon = \frac{\overline{T^m} - \overline{T^o}}{\overline{T^o}} \times 100\%, \quad (4)$$

$$\text{RMS} = \left( \frac{\sum_{i=1}^N (T_i^m - T_i^o)^2}{N} \right)^{1/2}. \quad (5)$$

For a particular depth,  $\overline{T^m}$ ,  $\overline{T^o}$  are the mean values (taken over 1999) of model-predicted and observed temperatures;  $R$  is the correlation between model-predicted and observed values;  $\sigma^{(m,o)}$  is the standard deviation for model or observed data;  $\varepsilon$  is the error in prediction of mean values, and RMS is the rms error of predictions. In Table 1, the values of parameters (2)–(5) at different depths for station M1 are given. The values of parameters for stations M2 and M4 for surface layer only are presented in Table 2. The correlations between model and observed SSTs for all stations are larger than 0.69. The model provides a fairly accurate prediction of the mean SST at M4 (an error of 0.27%). For the other two stations, the errors of mean SST predictions are 7.36% for M1 and 4% for M2. At the same time, the model SST variability is lower than the one observed (comparisons of  $\sigma^{(m,o)}$  in Tables 1 and 2). For deeper layers (Table 1), the errors of mean temperature predictions range from 3% to 16%. However, the model variability for the subsurface layers is comparable with the observed, and the RMS error decreases with depth. Yet, all the  $\varepsilon$  in Tables 1 and 2 are positive. This means that model temperatures are warmer than observed for all levels down to 300 m.

Table 3 presents the values of parameters (2)–(5) for model-predicted and observed salinity at the M1 station. The correlations between model and observed salinity are lower than the correlations between model and observed temperatures for the corresponding depths. One of the reasons for this

Observed and model SST, 6/12/95

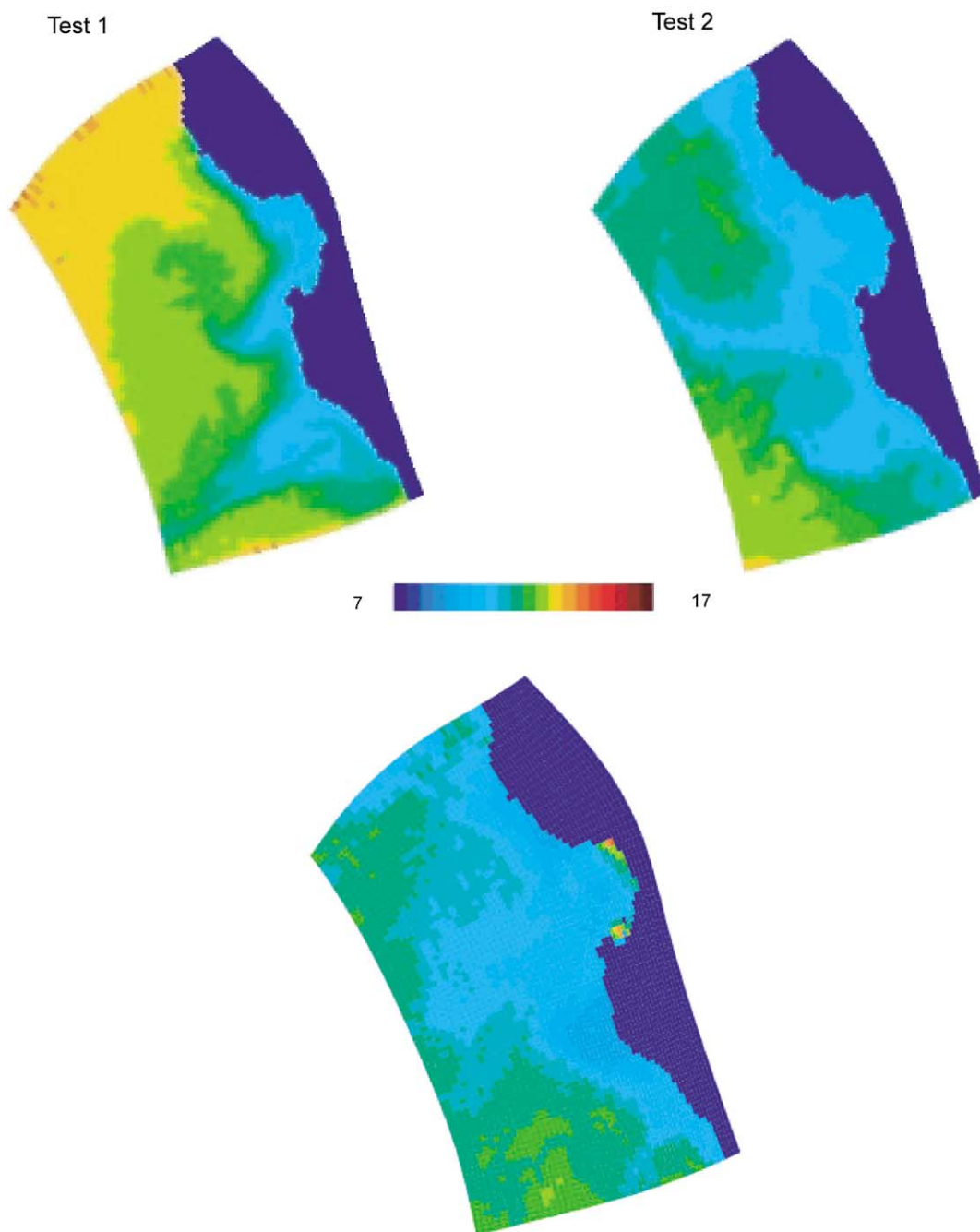


Fig. 3. Observed and model-predicted SST on 6/12/1995. Top left panel—model-predicted SST (Test 1); top right panel—model-predicted SST (Test 2); bottom panel—observed SST.

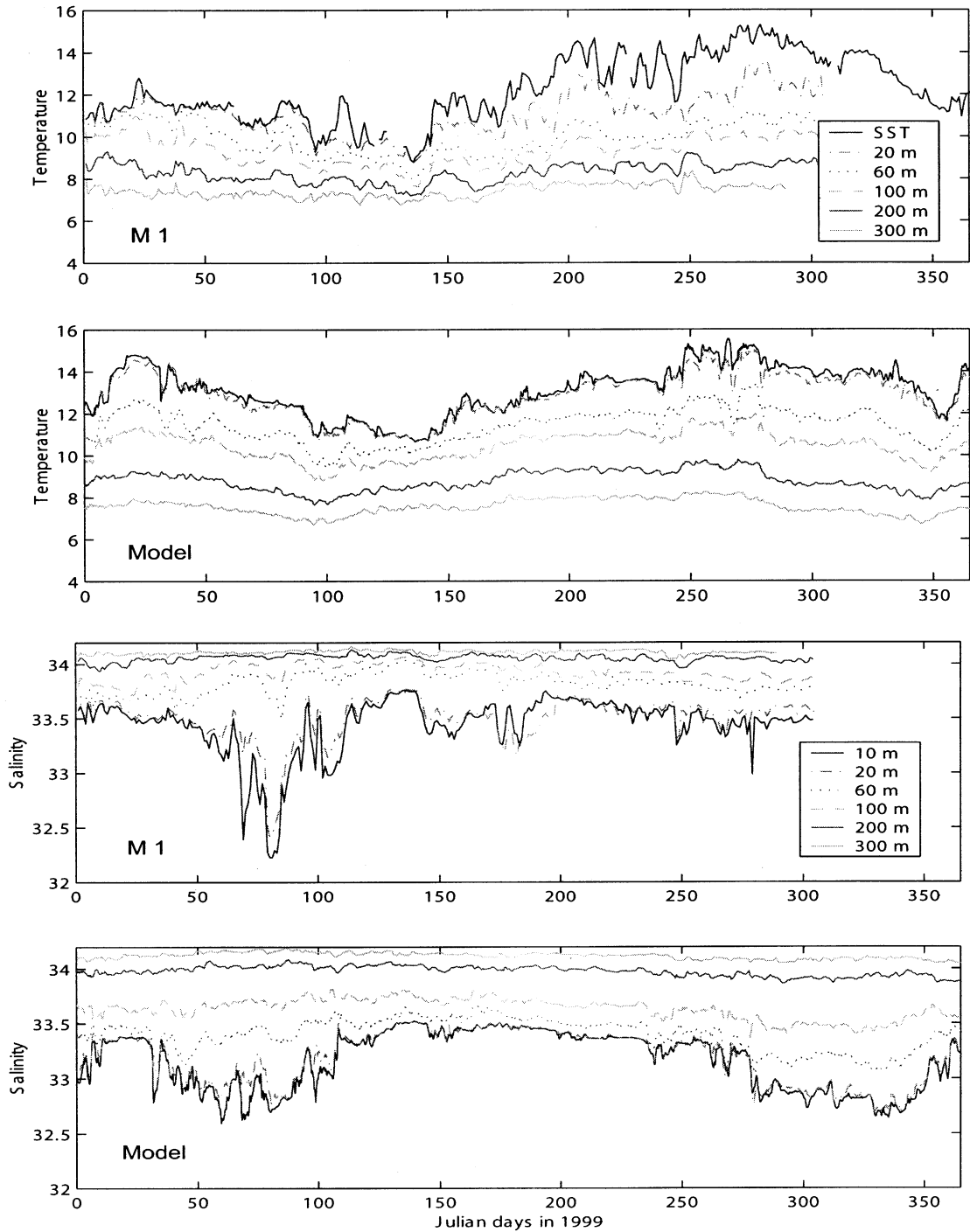


Fig. 4. Observed and model-predicted time series of temperature and salinity at M1 station.

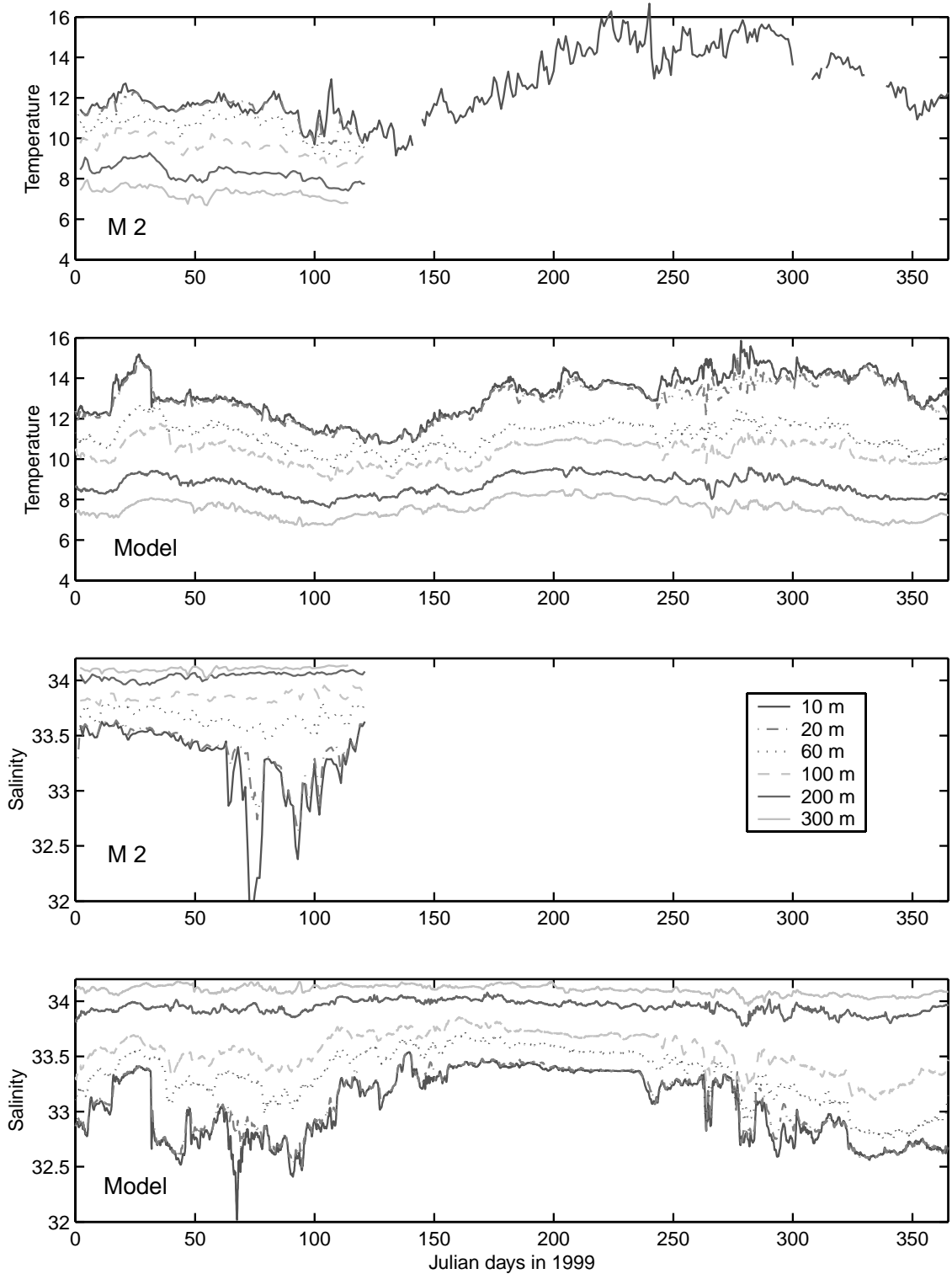


Fig. 5. Observed and model-predicted time series of temperature and salinity at M2 station.

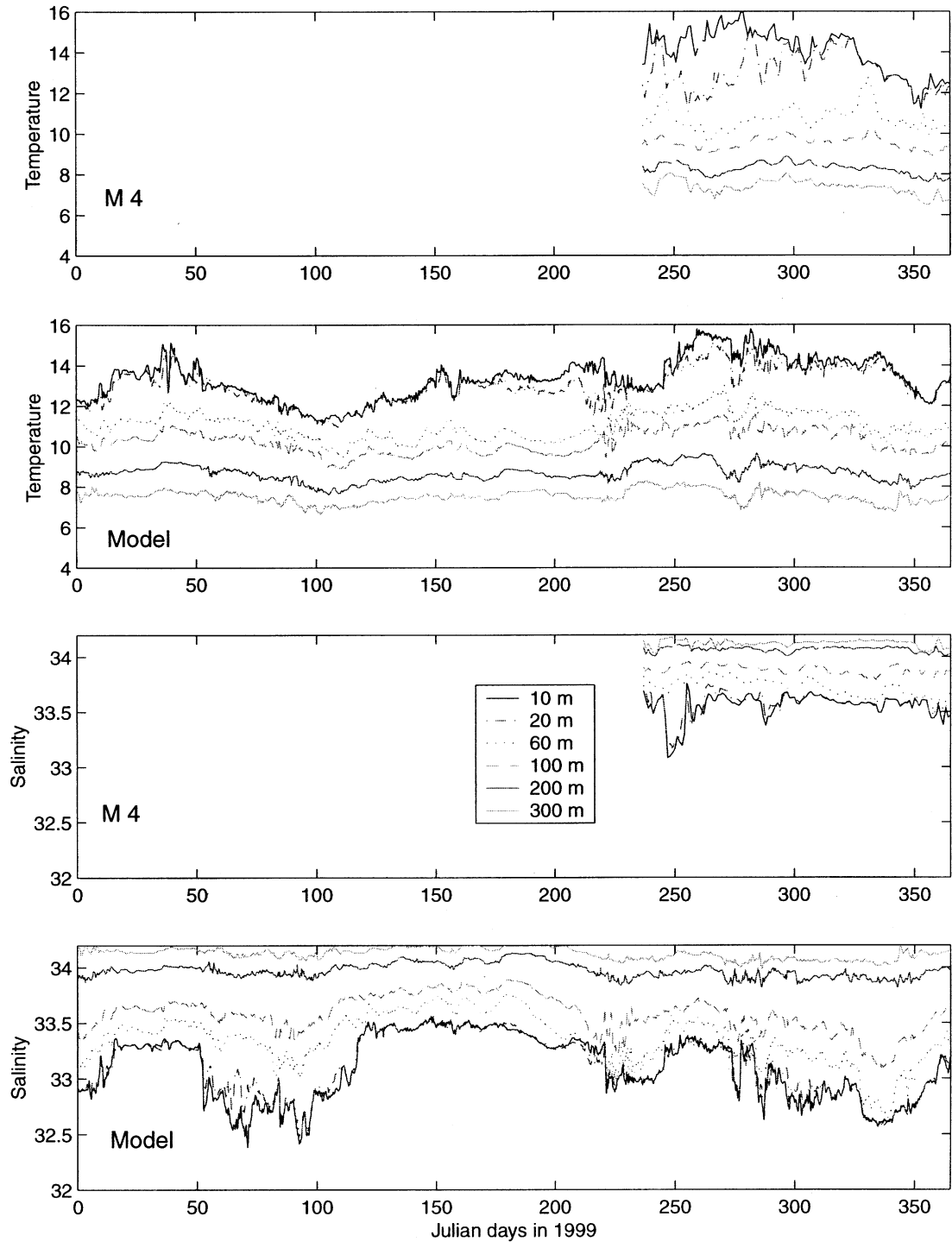


Fig. 6. Observed and model-predicted time series of temperature and salinity at M4 station.

Table 1  
Comparison of model-predicted and observed temperatures at M1 station

Depth	$R^a$	$\overline{T^m}$	$\sigma^m$	$\overline{T^o}$	$\sigma^o$	$\varepsilon$ (%)	RMS
0.00	0.77	13.15	1.12	12.25	1.52	7.36	1.33
20.00	0.84	12.84	1.12	11.10	1.03	15.68	1.85
60.00	0.76	11.46	0.83	9.98	0.81	14.88	1.59
100.00	0.73	10.51	0.69	9.33	0.70	12.60	1.28
200.00	0.60	8.86	0.47	8.28	0.46	7.03	0.72
300.00	0.66	7.66	0.35	7.41	0.30	3.29	0.38
With MCSST assimilation							
0.00	0.91	13.07	1.161	12.25	1.52	6.62	1.05
20.00	0.83	12.70	1.074	11.10	1.03	14.43	1.72
60.00	0.71	11.42	0.828	9.98	0.81	14.50	1.58
100.00	0.71	10.45	0.664	9.33	0.70	11.94	1.23
200.00	0.59	8.84	0.460	8.28	0.46	6.75	0.63
300.00	0.65	7.63	0.346	7.41	0.30	2.90	0.35

<sup>a</sup>For symbols, refer to Eqs. (2)–(5).

Table 2  
Comparison of model-predicted and observed sea surface temperatures at M2 and M4 stations

Stations	$R^a$	$\overline{T^m}$	$\sigma^m$	$\overline{T^o}$	$\sigma^o$	$\varepsilon$ (%)	RMS
M2	0.79	13.12	1.10	12.62	1.66	4.00	1.15
M4	0.69	14.11	0.88	14.07	1.08	0.27	0.81

<sup>a</sup>For symbols, refer to Eqs. (2)–(5).

Table 3  
Comparison of model-predicted and observed salinities at M1 station

Depth	$R^a$	$\overline{T^m}$	$\sigma^m$	$\overline{T^o}$	$\sigma^o$	$\varepsilon$ (%)	RMS
0.00	0.45	33.14	0.28	33.58	0.40	−1.30	0.58
20.00	0.39	33.25	0.21	33.50	0.20	−0.76	0.35
60.00	0.63	33.43	0.13	33.82	0.10	−1.16	0.41
100.00	0.71	33.66	0.09	33.93	0.08	−0.80	0.29
200.00	0.62	33.99	0.04	34.06	0.04	−0.19	0.11
300.00	0.44	34.13	0.03	34.11	0.02	0.05	0.09

<sup>a</sup>For symbols, refer to Eqs. (2)–(5).

is that the PWC model assimilates MCSST data and, thus produces better predictions of temperatures than salinities. At the same time, the errors in the prediction of mean values of salinity are smaller than those for temperatures. Also, in contrast to the temperature mean value predictions, the errors for salinity at the M1 station are negative down to 200 m, indicating that the

subsurface model water masses are fresher than those observed. Overall, the ICON model predictions indicate a need for heat and mass fluxes as surface forcing.

The observed temperatures in summer show persistent sizeable differences between the surface and 20 m depth (see Fig. 4) that indicate surface warming and the development of a shallow surface

mixed layer (shallower than 20 m). But in the model, the differences between surface and 20 m depth temperatures remain almost the same nearly all year. This means that the model mixed layer is thicker than observed during the summer and early fall.

Observed and model-predicted mixed layer depths (MLD) were estimated using the criteria and definitions of Martin (1985). Two MLD definitions were used: (a) the depth at which the water temperature becomes  $0.1^{\circ}\text{C}$  less than the model SST, and (b) the depth at which the water temperature becomes  $0.2^{\circ}\text{C}$  less than the model SST. As noted in Martin (1985), the latter criteria misses a few of the shallow, short-term, mixed layers.

The observed and model-predicted MLDs were averaged over July–September of 1999 for the M1 station and over September for the M4 station (M4 was not deployed until August of 1999). The averages are shown in Table 4. The observed MLDs indicate the development of a shallow surface mixed layer of  $<20$  m. However, the ICON model-predicted MLDs (second row in Table 4) are about twice as large as the observed MLDs.

Concerning these differences in the observed and predicted MLDs, we note that, without surface heat forcing, the model thermal vertical structure is going to be based on the vertical structure at the open boundaries and mixing within the domain acting on the vertical structure introduced at the open boundaries. In Table 4

(third row), the MLDs estimated from PWC predictions are shown. There is very good agreement between the observed and PWC-predicted mixed layer depths. This suggests that the simulations with the ICON model have resulted in over-mixing. Note, that the problems of over-mixing and the development of a deeper than observed mixed layer with the use of Mellor–Yamada turbulence closure sub-model were reported before (see, for example, the recent paper by Burchard, 2001). However, both models, ICON and PWC, use the same Mellor–Yamada scheme with the same parameters. In the vertical, both models have the same resolution in sigma coordinates. At the M4 location, where the ICON and PWC model depths are 1936 and 2116 m respectively, the vertical resolution for the top 25–30 m is almost the same for both models: 0.96, 3.9, 8.7, 15.5, 24.2 and 33.9 m for the ICON model and 1.06, 4.2, 9.5, 16.9, 26.4 and 37.0 for the PWC model.

Several factors may be responsible for the over-mixing by the ICON model. For example, the ICON model has a higher horizontal resolution (1–4 km) than the PWC model (10 km). Therefore, smaller-scale processes are better resolved with the ICON model, and this could possibly lead to increased variability and over-mixing. As was mentioned before, the PWC model assimilates daily MCSST data by using a simple nudging technique with a time scale of 1 day. This can affect the MLD development in the PWC model. To explore the effect of direct assimilation of MCSST on the ICON model MLD predictions, we conducted an additional ICON simulation with the assimilation of MCSST fields. The assimilation was conducted using the same nudging technique as that employed in the PWC model. In Table 1, bottom panel, the values of parameters (2)–(5) at the M1 station location are presented for the model run with MCSST data assimilation. Comparisons between this run and the run without assimilation indicate the improvement of the model predictions as a result of MCSST assimilation. The correlation between model and observed SSTs are improved, and the model mixed layer during the summer time is shallower than in the case without assimilation (see Table 4, fourth row).

Table 4  
Observed and model-predicted mixed layer depths (MLD) in m

	M1		M4	
	$0.1^{\circ}\text{C}$	$0.2^{\circ}\text{C}$	$0.1^{\circ}\text{C}$	$0.2^{\circ}\text{C}$
Observed	10.8	11.6	12.6	13.2
ICON model	24.1	29.0	19.2	21.7
PWC model	11.0	15.4	10.7	13.8
ICON model W/assimilation of MCSST	18.3	22.9	18.2	22.1
ICON model W/COAMPS wind stress	24.4	28.6	25.1	29.1
ICON model W/COAMPS wind stress and heat fluxes	12.8	14.0	14.7	17.1

However, the assimilation of MCSST data does not compensate adequately for the over-mixing in the model. With the inclusion of different heat fluxes (especially evaporative heat flux) we can expect that the ICON model could produce a thinner and sharper surface mixed layer than without the use of heat fluxes.

To investigate this, we conducted experiments with the use of air–sea fluxes from the 9-km-resolution COAMPS atmospheric model (Hodur, 1997). First, the estimates of MLD of the ICON model forced with only wind stresses from COAMPS predictions are shown in Table 4 (fifth row). As expected, the increase in resolution of the wind forcing does not improve the ICON model MLD predictions; moreover, the mixed layer at the M4 location become even slightly deeper than in the case with coarse-resolution wind forcing (see Table 4, second row). In the next experiment, heat fluxes from COAMPS predictions were applied as the ICON model surface boundary conditions following the Zavatarelli and Mellor (1995) scheme.

The following components of surface heat flux from the COAMPS atmospheric model predictions were used: short-wave radiation ( $Q_s$ ), long-wave radiation ( $Q_l$ ), sensible heat flux ( $Q_h$ ), and latent heat flux ( $Q_e$ ). The following surface boundary condition for temperature was used:

$$K_h \left( \frac{\partial T}{\partial z} \right) = (1 - T_r) Q_s + Q_l + Q_h + Q_e, \quad (6)$$

where  $T_r$  is the transmission coefficient. The remainder of the short-wave radiation  $R = Q_s T_r \exp(-\lambda z)$ , (where  $\lambda$  is the attenuation coefficient and  $z$  is the depth) is attenuated to the water column by addition of the term  $\partial R / \partial z$  to the right side of the model equation for temperature. Values of  $T_r = 0.31$  and  $\lambda = 0.042 \text{ m}^{-1}$  were used (Zavatarelli and Mellor, 1995).

The estimates of MLD for the ICON model predictions forced with COAMPS heat fluxes are shown in Table 4 (sixth row). There is a significant improvement in the model mixed layer depth predictions with the inclusion of heat fluxes. While in the regional PWC model, assimilation of SST data might be enough for the development of a correct vertical thermal structure, in the finer-

resolution coastal ICON model, the variable heat fluxes are needed as surface boundary conditions for the accurate prediction of the vertical thermal structure. In the future, we are planning to investigate the influence of the transmission and attenuation coefficients' values, as well as the numerical scheme of surface heat fluxes' application.

As mentioned in the introduction, the major flow regimes featured in the Monterey Bay area are the shallow, equatorward, broad CC and the two narrow poleward-flowing boundary currents within about 150 km of the coast: the CU and the IC (Lynn and Simpson, 1987; Ramp et al., 1997; Collins et al., 2000). The northward flow associated with the CU is predominately at 200 m over the continental slope off the Monterey Bay. The IC is a shallow seasonal flow, appearing in fall and winter.

As stated in Collins et al. (2000), the upper 1000 m depth-averaged mean velocity pattern clearly indicates the extent of poleward flow associated with inshore currents. They reported that four stations along  $36.33^\circ$  of latitude (at 33–65 km from shore, between  $122.25^\circ\text{W}$  and  $122.6^\circ\text{W}$  of longitude) show west-northwestward ( $290^\circ$ – $310^\circ\text{T}$ ) mean flow of 3.7–5.3 cm/s. Their estimates were based on 19 cruises conducted from April 1988 to April 1991. The ICON model mean flow over the upper 1000 m for July–December 1999 was estimated along the line connecting the four inshore stations of Collins et al. (2000). The ICON model mean flow shows a northwestward direction at  $308^\circ\text{T}$  with intensity of 3.13 cm/s, which is in good agreement with the findings in Collins et al. (2000).

In Figs. 7–10, the model-predicted velocities for different depths (0, 40, 100 and 350 m) are presented for the period January 1–4, 1999. On January 1, 1999 (Fig. 7), there is no northward flow along the coast at the surface. However, the subsurface northward flow exists in the southern portion of the domain. At 350 m, there is evidence of a northward flow along the coast. However, the next day (January 2, Fig. 8), a northward flow appears at the surface in the southern portion of the domain, and this northward flow is stronger for all depths in comparison to the flow on

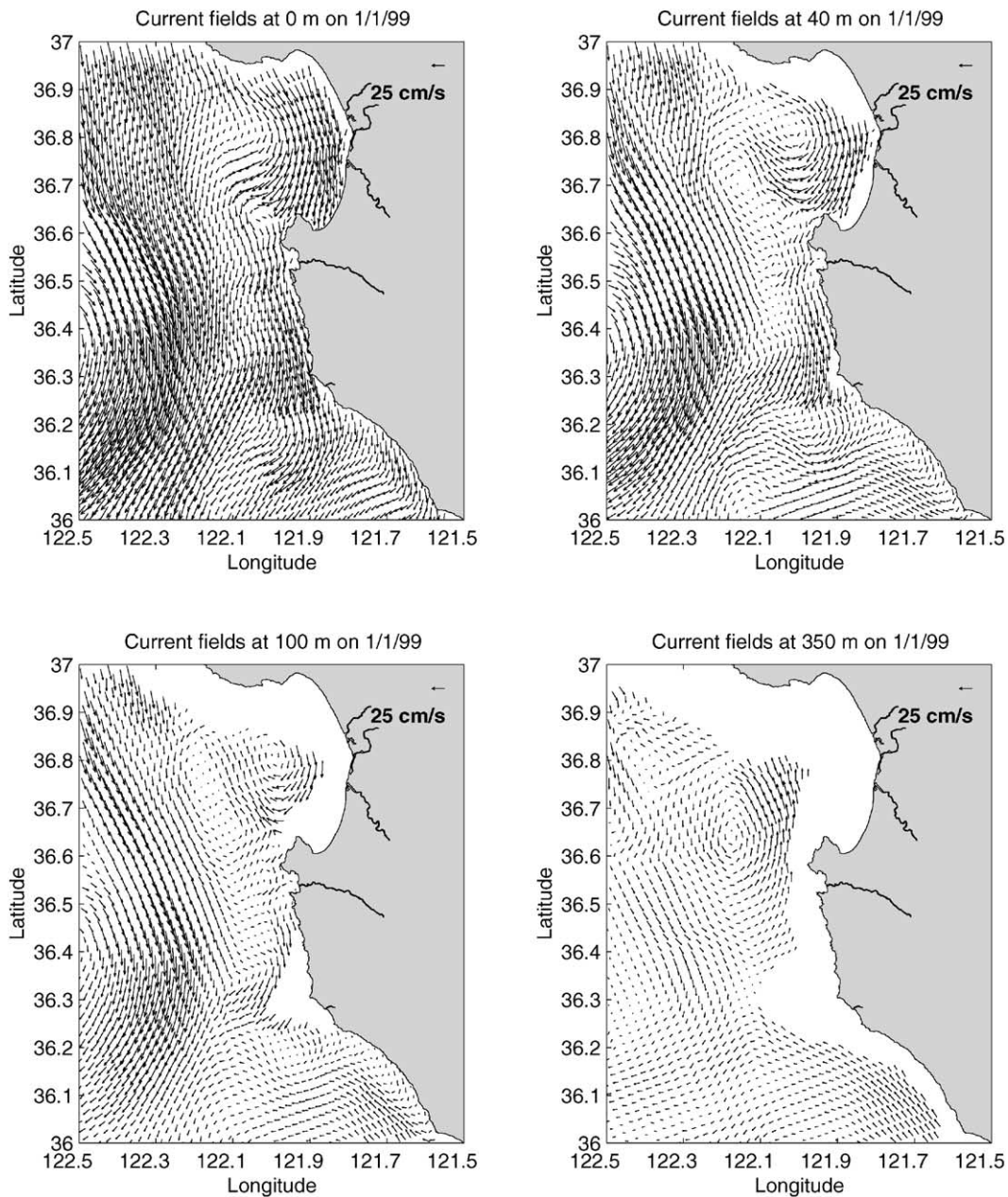


Fig. 7. Model-predicted currents at surface, 40, 100 and 350 m depth on 1/1/1999.

January 1. As time progresses (Figs. 9 and 10), the northward flow for all levels becomes stronger. NOGAPS wind stresses used to force the model during these days are shown in Fig. 11. Due to wind blowing from north to south (Fig. 11) during

January 1 and 2 and then weakening during January 3 and 4, the intensification of the northward flow is a result of the influence of the open boundary currents coming from the PWC model, and this northward intensified flow represents the

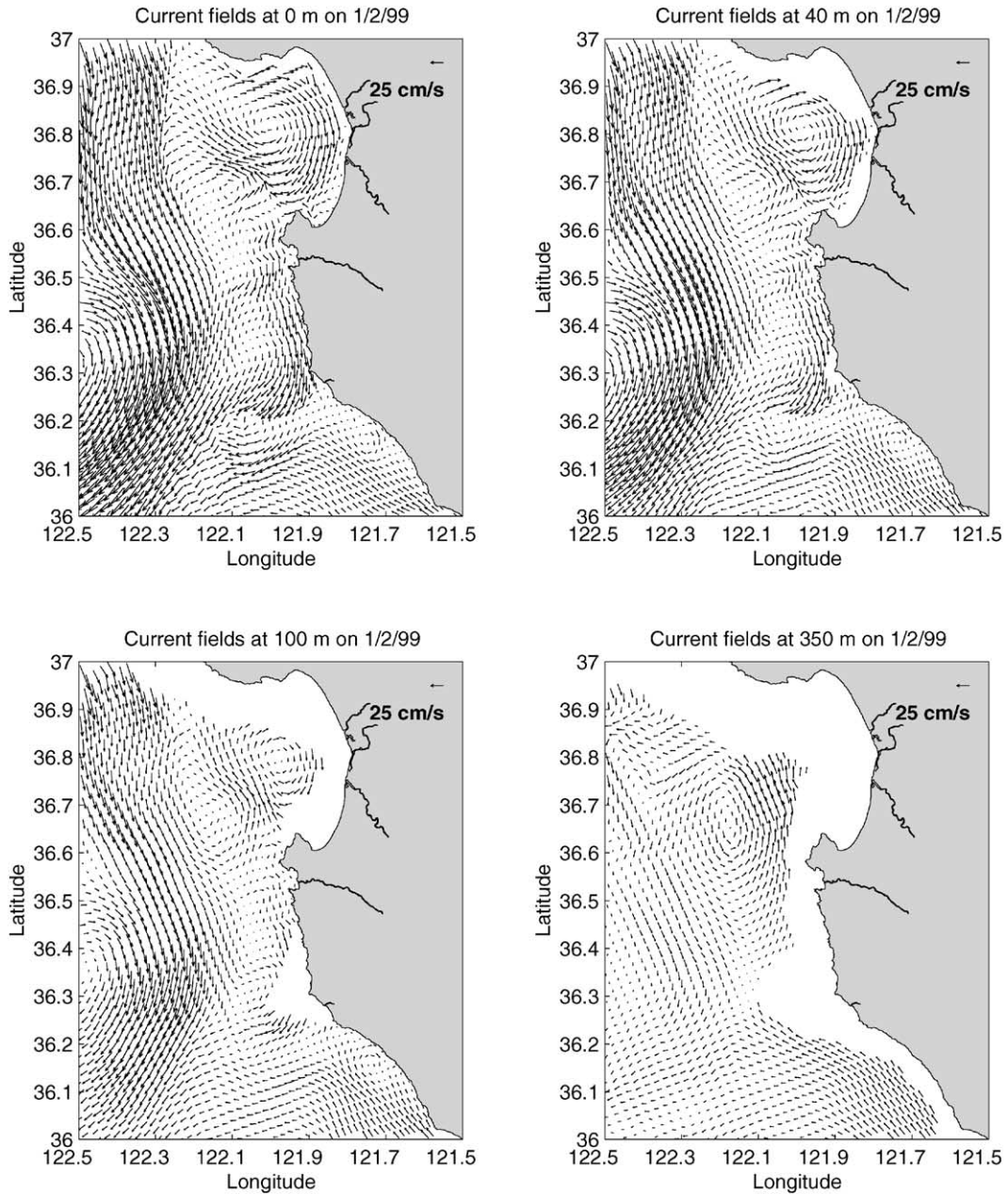


Fig. 8. The same as in Fig. 7 on 1/2/1999.

IC and CU currents. The fact that the model shows intensification and shallowing of the CU and IC currents during the fall and winter is in good agreement with observations (Collins et al., 2000).

On January 2 and 3 (Figs. 8 and 9), the model-predicted currents on the surface and subsurface down to 100 m depth show an anticyclonic eddy in the Bay with a much weaker, however intensified with the depth, cyclonic

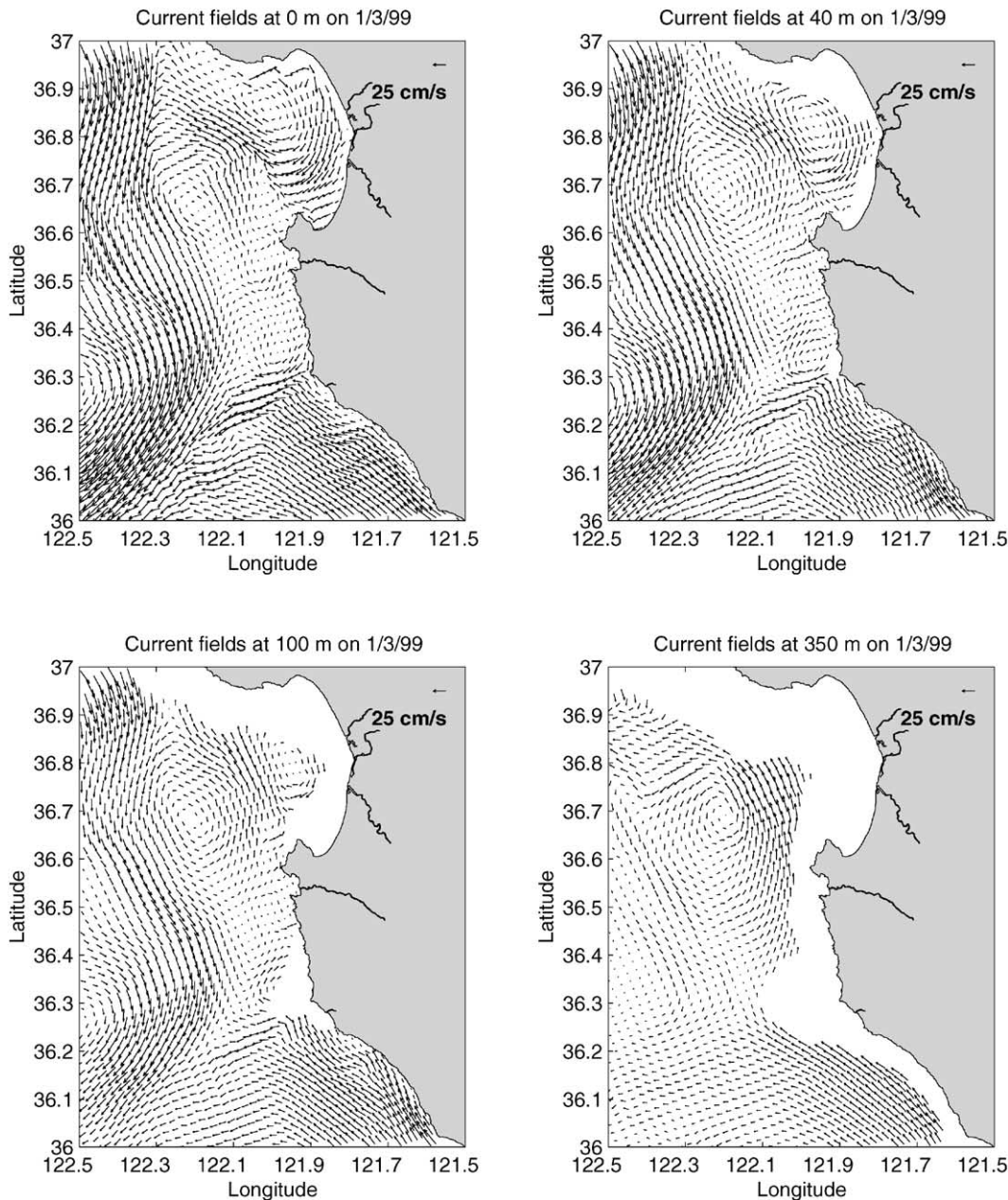


Fig. 9. The same as in Fig. 7 on 1/3/1999.

eddy on its offshore side. This structure propagates from the bottom to the top of the water column. Observed CODAR surface currents on January 2 and 3, 1999 (Fig. 12) also show an anticyclonic eddy in the Bay. Note that, the model

does not have an anticyclonic eddy on the surface on January 1, but the anticyclonic-cyclonic structure already exists at 40 m (Fig. 7). This gives the idea that the anticyclonic-cyclonic structure is probably a result of an interaction

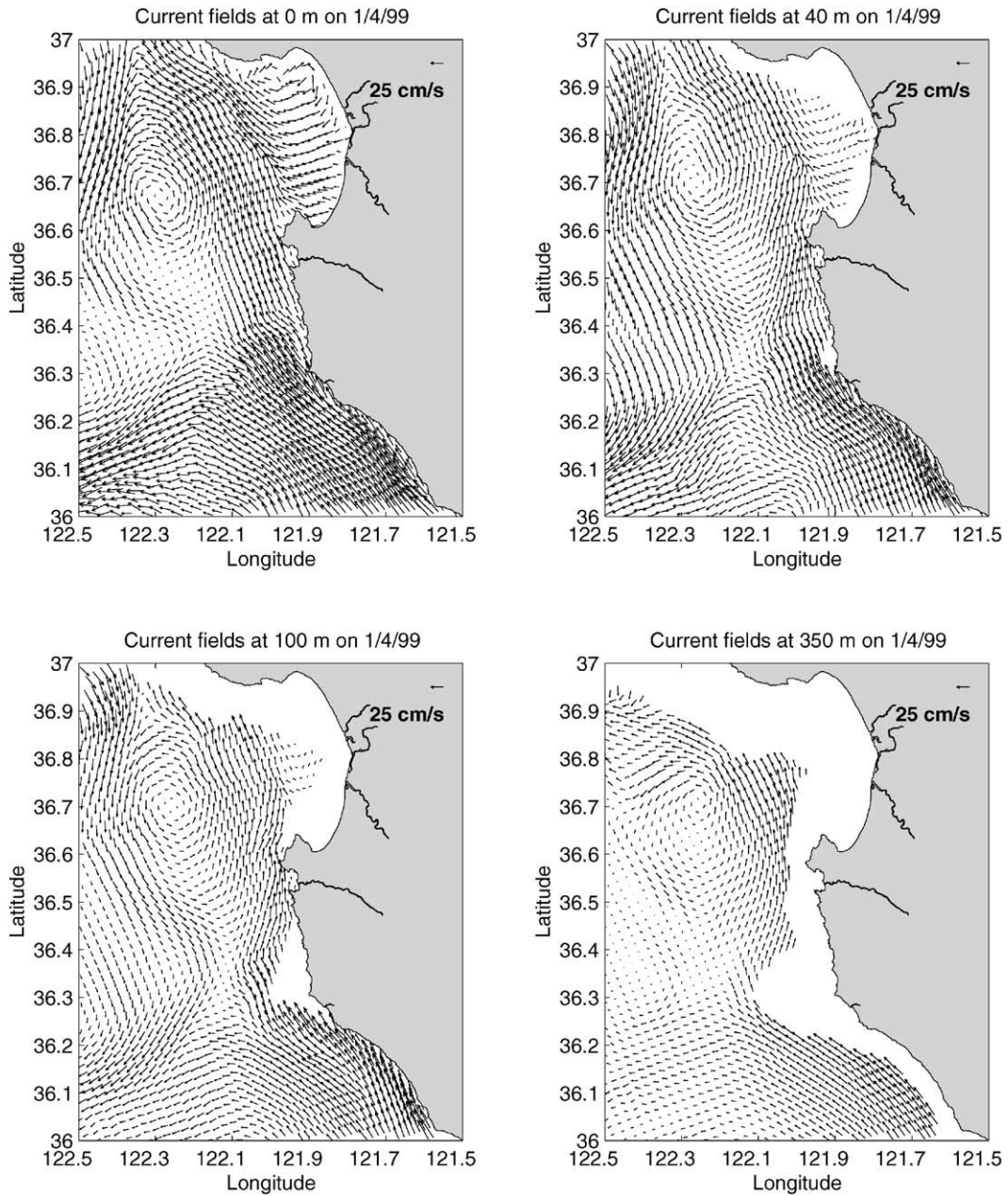


Fig. 10. The same as in Fig. 7 on 1/4/1999.

between surface and subsurface flow forced by wind blowing from north to south and the intensification and shallowing of the IC flowing from south to north. With the weakening of the southward wind (Fig. 11, January 3 and 4) and

intensification of northward flow, the anticyclonic eddy disappears in the Bay on January 4 (the flow is mostly northward), in agreement with the observed CODAR surface currents (Fig. 12, bottom right panel).

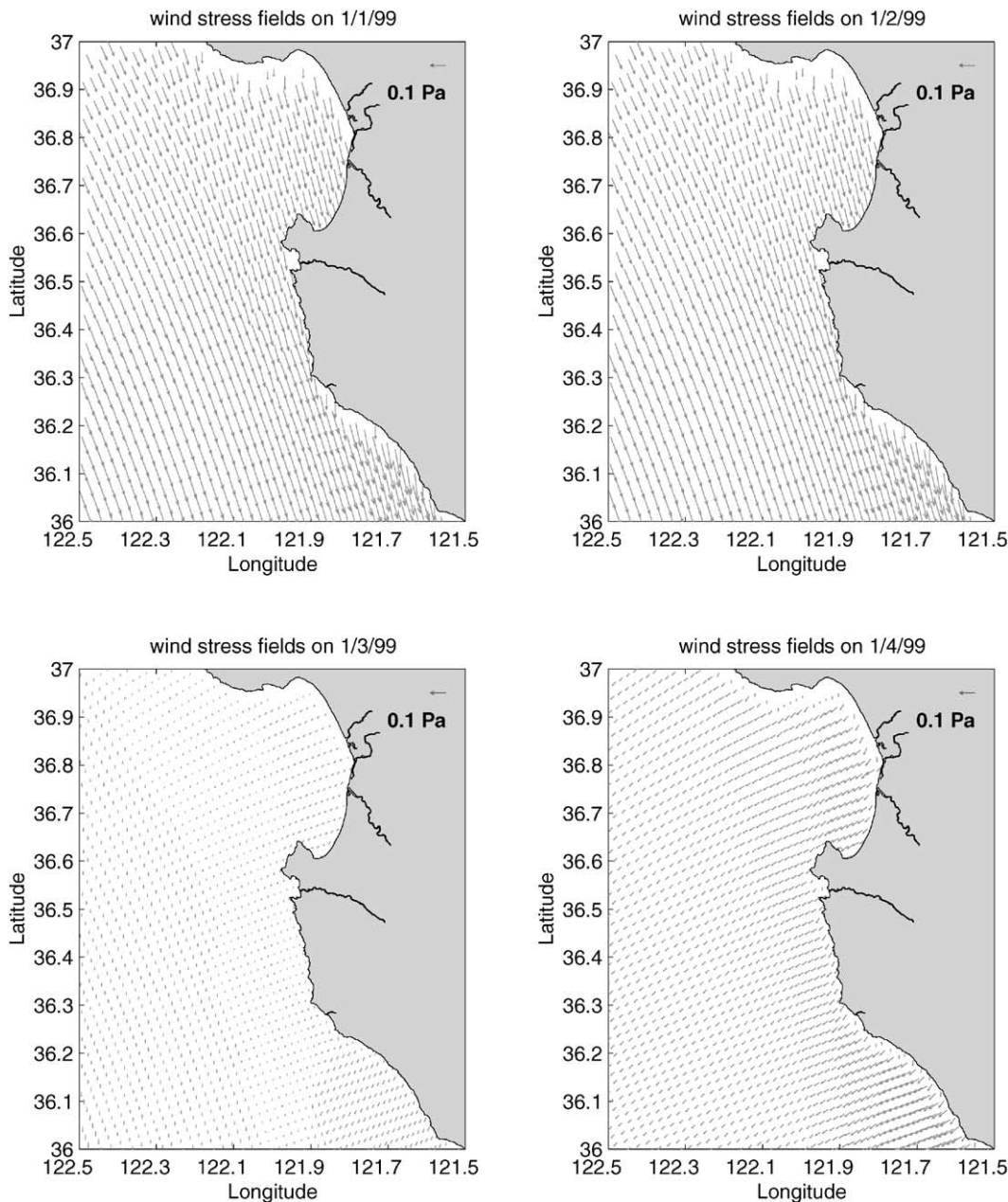


Fig. 11. FNMOC NOGAPS wind stresses for 1/1-1/4 of 1999.

**5. Discussion and future model development plan**

The numerical modeling of the Monterey Bay area, characterized by a complex coast-line, steep topography with depth reaching 3500 m within

100 km offshore, and influenced by phenomena of the CC System, is a very challenging task.

The ICON model configuration consists of the following major components: three-dimensional, prognostic primitive-equation model (POM), a

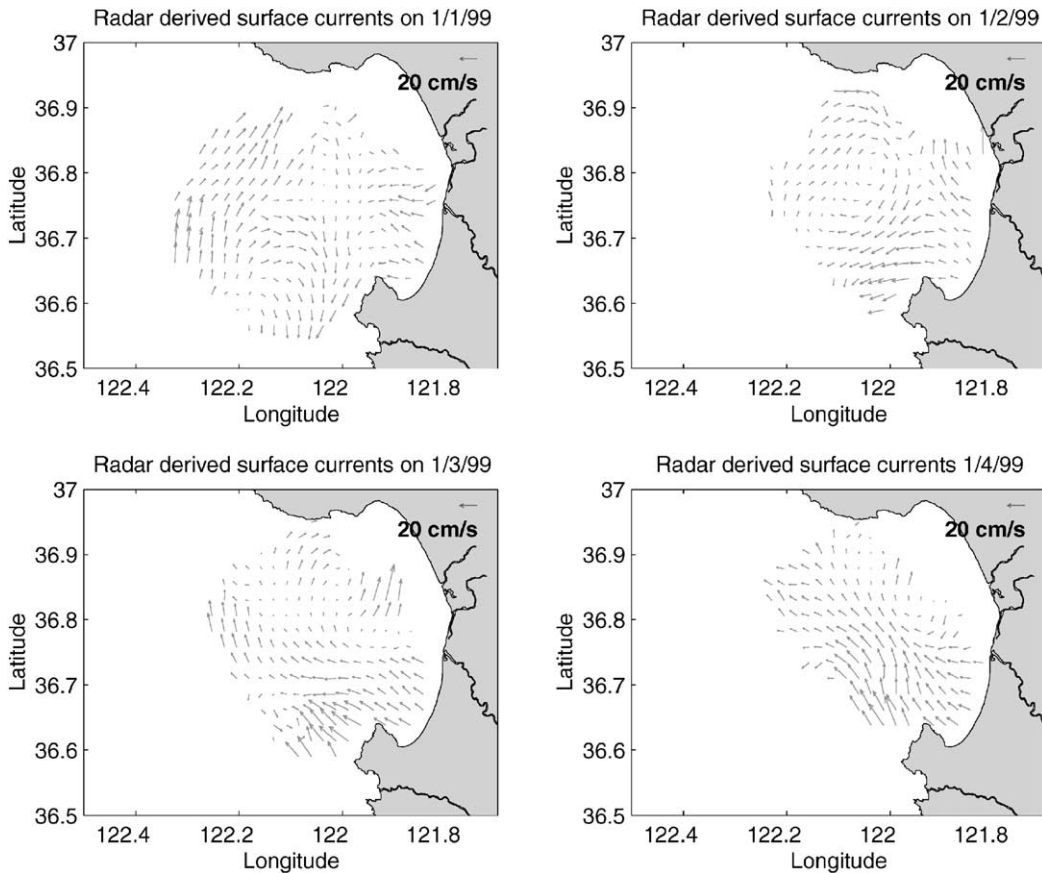


Fig. 12. CODAR-derived surface currents for 1/1-1/4 of 1999.

curvilinear orthogonal grid with open boundaries being orthogonal to the major bathymetric features on the open boundaries, barotropic and baroclinic coupling on the open boundaries with the larger-scale model, and atmospheric forcing from state-of-the-art Navy atmospheric models. The influence of different ICON model components on reproducing major hydrographic conditions observed in the Monterey Bay area has been analyzed. These hydrographic conditions simulated by the model include cool plumes of upwelled water extending from north to south and seaward of the Monterey Bay during upwelling season; a meandering, alongshore ocean front between the upwelled water and the warmer water of the CC; two narrow poleward-flowing boundary currents associated with the CU, and the shallow IC. Also,

the model does well in reproducing the mean water temperatures and salinities at a given depth and shows a high correlation between observed and model temperatures for different levels.

The model predictions demonstrated the significance and importance of the ICON coupling with the larger-scale PWC model for reproducing major flow regimes and hydrographic conditions in the area. Without coupling to PWC model, the average angles between the ICON model and observed ADCP currents at M2 mooring location are larger than  $100^\circ$  for the top 120 m. The ICON coupling with the PWC model gives an almost zero average angle between the ICON model currents and observations, which is a significant improvement in the ICON model predictions in comparison to the case without coupling.

Most existing radiation-type open boundary conditions work well in the case when flow is almost orthogonal to the open boundaries (the tangential component is not significant). However, for coastal limited-area models, the tangential component of flow can be significant if the open boundaries are oriented parallel to the longitude and latitude (for cartesian, rectangular grids). In this case, specification of the tangential component of the flow, with or without the use of extraneous information (for example, from a larger-scale model) can introduce significant unrealistic currents around the open boundaries. The choice of cross-shelf open boundaries to be near-orthogonal to the isobaths of the bathymetry played an important role in the successful transition of PWC information into the ICON model domain and avoiding the build-up of unrealistic currents around the open boundaries.

Analysis of the ICON model mixed layer predictions demonstrated that the model needs the inclusion of surface heat fluxes for accurate prediction of the shallowing mixed layer during the summer time (see Table 4). The ICON and PWC models are based on the same Blumberg and Mellor (1987) model and use the same turbulence closure sub-model developed by Mellor and Yamada. The coarser-resolution PWC model predictions with assimilation of the MCSST data demonstrated the development of the shallow mixed layer, in better agreement with observations, than the mixed layer developed in the finer-resolution ICON model predictions with assimilation of the same MCSST data set. This suggests that the over-mixing in the model may occur when we move from a coarser resolution regional model to the finer-resolution coastal model (which is reasonable because a finer-resolution leads to more variability), and that while in regional models assimilation of SST data might be enough for the development of a correct vertical thermal structure, in finer-resolution coastal models the variable heat fluxes are needed as surface boundary conditions for the accurate prediction of the vertical thermal structure.

The future development of the ICON model will be focused on model ability to assimilate different types of observational data (HF radar data

(CODAR), mooring data, Lagrangian drifters, etc.), as well as improvement of the air–sea interaction and coupling schemes in the model.

### Acknowledgements

This work was supported by the National Oceanographic Partnership Program. We would like to thank D.-S. Ko for substantial help with the PWC model and useful discussions of the model results. Also, we would like to thank P. Rochford, S. Derada and S. Cayula for providing PWC model data and atmospheric forcing in 1998, 1999. We would like to thank F. Chavez for providing M1 and M2 mooring data, F. Bahr and M. Cook provided able assistance with the quality-control, processing, and presentation of the mooring and CODAR data, respectively. Computer time was provided in part by grants of HPC time from the DoD HPC Centers at: US Naval Oceanographic Office, Stennis Space Center, Mississippi; US Army Corps. of Engineers Waterways Experiment Station (CEWES).

### References

- Blumberg, A.F., Mellor, G.L., 1987. A description of a three-dimensional coastal ocean circulation model. In: Heaps, N.S. (Ed.), *Coastal and Estuarine Sciences 4: Three Dimensional Coastal Models*. AGU, Washington, DC, pp. 1–16.
- Burchard, H., 2001. On the  $q^2l$  equation by Mellor and Yamada (1982). *Journal of Physical Oceanography* 31, 1377–1387.
- Clancy, R.M., deWitt, P.W., May, P., Ko, D.-S., 1996. Implementation of a coastal ocean circulation model for the west coast of the United States, *Proceedings of the American Meteorological Society Conference on Coastal Oceanic and Atmospheric Prediction*, Atlanta, G.A., pp. 72–75.
- Collins, C.A., Garfield, N., Rago, T.A., Rishmiller, F.W., Carter, E., 2000. Mean structure of the inshore counter-current and California undercurrent of Point Sur, California. *Deep-Sea Research II* 47, 765–782.
- Flather, R.A., 1976. A tidal model of the northwest European continental shelf. *Memorie Societa Reale Scienze Liege* 6 (10), 141–164.
- Hodur, R.M., 1997. The naval research laboratory's coupled ocean/atmosphere mesoscale prediction system (COAMPS). *Monthly Weather Review* 125, 1414–1430.

- Ko, D.-S., Allard R.A., Metzger, E.J., Rhodes, R.C., 1996. A Coupled West Coast Model With Seasonal Forcing, *Eos* 76 (Suppl. 3), OS38.
- Kundu, P.K., 1976. Ekman veering observed near the ocean bottom. *Journal of Physical Oceanography* 6, 238–242.
- Lewis, J.K., Shulman, I., Blumberg, A.F., 1998. Assimilation of CODAR observations into ocean models. *Continental Shelf Research* 18, 541–559.
- Lipphardt, B.L., Kirwan, A.D., Grosch, C.E., Ivanov, L., Lewis, J.K., 1997. Merging disparate ocean data. In: Pouliquen, E., Kirwan, A.D., Pearson, R.T. (Eds.), *Rapid Environmental Assessment*, NATO SACLANT Undersea Research Center, La Spezia, Italy, pp. 211–218.
- Lipphardt, B.L., Kirwan, A.D., Grosch, C.E., Lewis, J.K., Paduan, J.D., 2000. Blending HF radar and model velocities in Monterey Bay through normal mode analysis. *Journal of Geophysical Research* 105, 3425–3450.
- Ly, L.N., Luong, P., Paduan, J.D., Karacin, D., 1999. Response of the Monterey Bay Region to Wind Forcing by an Atmospheric Model. *Proceedings of the 3rd Conference on Coastal Atmospheric and Oceanic Prediction and Processes*, New Orleans, LA, pp. 76–79.
- Lynn, R.J., Simpson, J.J., 1987. The California current system: the seasonal variability of its physical characteristics. *Journal of Geophysical Research* 92, 12,947–12,966.
- Martin, P.J., 1985. Simulations of the mixed layer at OWS November and Papa with several models. *Journal of Geophysical Research* 90, 903–916.
- Paduan, J.D., Rosenfeld, L.K., 1996. Remotely sensed surface currents in Monterey Bay from shore-based HF radar (Coastal Ocean Dynamics Application Radar). *Journal of Geophysical Research* 101, 20,669–20,686.
- Petruncio, E.T., 1996. Observations and modeling of the internal tide in a submarine canyon, Ph.D. Thesis, Naval Postgraduate School, Monterey, CA, 181pp.
- Petruncio, E.T., Rosenfeld, L.K., Paduan, J.D., 1998. Observations of the internal tide in Monterey Canyon. *Journal of Physical Oceanography* 28, 1873–1903.
- Ramp, S.R., Rosenfeld, L.K., Tisch, T.D., Hicks, M.R., 1997. Moored observations of the current and temperature structure over the continental slope off central California. 1. A basic description of the variability. *Journal of Geophysical Research* 102, 22,877–22,902.
- Righi, D.D., Strub, P.T., Kindle, J.C., 1999. Validation of a California current model through comparison with altimeter and drifter circulation statistics. *Proceedings of the 3RD Conference on Coastal Atmospheric and Oceanic Prediction and Processes*, New Orleans, L.A., pp. 97–100.
- Rochford, P.A., Shulman, I., 2000. Boundary Conditions in the Pacific West Coast Princeton Ocean Model of CoBALT. *NRL Technical Report*, NRL/MR/7330-00-8245, 18pp.
- Rosenfeld, L.K., Schwing, F.B., Garfield, N., Tracy, D.E., 1994. Bifurcated flow from an upwelling center: a cold water source for Monterey Bay. *Continental Shelf Research* 14, 931–964.
- Rosenfeld, L.K., Paduan, J.D., Petruncio, E.T., Concalves, J.E., 1999. Numerical simulations and observations of the internal tide in a submarine canyon. *Proceedings 'Aha Huliko'a Hawaiian Winter Workshop'*, University of Hawaii at Manoa, pp. 1–8.
- Shulman, I., Wu, C.-R., Lewis, J.K., Paduan, J.D., Rosenfeld, L.K., Ramp, S.R., Cook, M.S., Kindle, J.C., Ko, D.-S., 1999. Development of the high resolution, data assimilating numerical model of the Monterey Bay. *Proceedings of the 3RD Conference on Coastal Atmospheric and Oceanic Prediction and Processes*, New Orleans, L.A., pp. 232–235.
- Zavatarelli, M., Mellor, G.L., 1995. Numerical study of the Mediterranean Sea circulation. *Journal of Physical Oceanography* 25, 1384–1414.